

Crack Front Segmentation and Facet Coarsening in Mixed-Mode Fracture

Chih-Hung Chen,^{1,*} Tristan Cambonie,² Veronique Lazarus,² Matteo Nicoli,¹ Antonio J. Pons,³ and Alain Karma^{1,†}

¹Physics Department and Center for Interdisciplinary Research on Complex Systems,
Northeastern University, Boston, Massachusetts 02115, USA

²Laboratoire FAST, Univ Paris Sud, CNRS, Université Paris-Saclay, F-91405 Orsay, France

³Department of Physics, Polytechnic University of Catalonia, Terrassa, Barcelona 08222, Spain

(Received 17 September 2015; revised manuscript received 20 November 2015; published 30 December 2015)

A planar crack generically segments into an array of “daughter cracks” shaped as tilted facets when loaded with both a tensile stress normal to the crack plane (mode I) and a shear stress parallel to the crack front (mode III). We investigate facet propagation and coarsening using *in situ* microscopy observations of fracture surfaces at different stages of quasistatic mixed-mode crack propagation and phase-field simulations. The results demonstrate that the bifurcation from propagating a planar to segmented crack front is strongly subcritical, reconciling previous theoretical predictions of linear stability analysis with experimental observations. They further show that facet coarsening is a self-similar process driven by a spatial period-doubling instability of facet arrays.

DOI: 10.1103/PhysRevLett.115.265503

PACS numbers: 62.20.M-, 46.15.-x, 46.50.+a

Crack propagation is a main mode of materials failure. Understanding and controlling this complex phenomenon continues to pose both fundamental and practical challenges. While quasistatic planar crack growth with a tensile stress normal to the fracture plane (mode I) is well understood, geometrically much more intricate crack patterns can form in varied conditions [1]. A few examples include thermal or drying stresses that can cause cracks to oscillate and branch [2,3], or reorganize into complex three-dimensional patterns [4–6], nonlinear elastic effects that can induce crack front instabilities even in mode I [7], or the superposition of mode I and a shear stress parallel to the crack front (mode III). This mixed-mode I + III fracture is observed in a wide range of engineering and geological materials to produce arrays of daughter cracks, which are shaped as tilted facets and form by a geometrically complex crack front segmentation process [8–23].

Recent theoretical progress has been made to characterize the crack front instability leading to segmentation [24,25] and to describe the propagation of daughter-crack arrays [26]. However, theory and experiments have not produced a consistent picture. Griffith’s energetic criterion [27] predicts that planar crack growth is possible when the elastic energy release rate

$$G = \frac{1}{2\mu} [(1-\nu)K_I^2 + K_{III}^2] \quad (1)$$

exceeds a critical material-dependent threshold G_c , where K_I and K_{III} are the mode I and mode III stress intensity factors (SIFs), respectively, which characterize stress divergences near the crack front, μ is the shear modulus, and ν is Poisson’s ratio. Phase-field simulations have revealed that planar growth is linearly unstable against helical deformations of the crack front [24], and linear stability analysis in

the framework of linear elastic fracture mechanics (LEFM) [25] has predicted that this instability occurs when K_{III}/K_I exceeds a threshold

$$\left(\frac{K_{III}}{K_I}\right)_c = \sqrt{\frac{(1-\nu)(2-3\nu)}{3(2-\nu) - 4\sqrt{2}(1-2\nu)}}. \quad (2)$$

However, paradoxically, crack front segmentation is experimentally observed for K_{III}/K_I values much smaller than this threshold [8,23] or even vanishingly small [22]. Also poorly understood is “facet coarsening”, the progressive increase of facet width and spacing with propagation length from the parent crack.

In this Letter, we investigate both facet propagation and coarsening by mixed-mode I + III fracture experiments that allow us to visualize *in situ* complex crack morphologies during quasistatic propagation, thereby providing much more detailed geometrical information on crack front evolution than conventional postmortem fractography. Moreover, we model those experiments numerically with a phase-field approach. Fracture in this model has been shown to be governed by standard crack propagation laws assumed in the LEFM theory in the limit where the microscopic process zone around the crack front is much smaller than all other dimensions [28], namely, Griffith’s criterion and vanishing mode II SIF [29]. Therefore, the present phase-field simulations allow us to answer the nontrivial question of whether subcritical crack propagation observed experimentally for $K_{III}/K_I < (K_{III}/K_I)_c$ is described by the LEFM theory. This question could not be answered by linear stability analysis, confined to small-amplitude in- and out-of-plane perturbations of the crack front [25], or previous simulations that focused on supercritical crack propagation [24]. The results show unambiguously that subcritical crack

propagation is quantitatively described by the LEFM theory and shed new light on the secondary instability of facet arrays underlying the coarsening process.

Experiments are carried out using Plexiglas beams and a traditional three- or four-point bending setup [30]. To introduce some amount of mode III, the initial planar notch in the sample is tilted at an angle from the mode I central plane of symmetry [19,39]. A special procedure is used to initiate a sharp crack with a straight front [30]. The corresponding values of the SIF for each angle and hence K_{III}/K_I have been obtained by finite element calculations, which show that K_{III}/K_I varies between approximately 0.1 and 0.5 when the notch angle varies between 15° and 45° , where zero angle corresponds to pure mode I loading. Several beams were broken by fatigue in the bending setup [30]. The advantage of this cyclic type of loading is that the crack advance (i) is quasistatic, while leaving the crack path unchanged in comparison to the one obtained under monotonical increasing loading [40], and (ii) controlled by the number of cycles so that complex crack morphologies can be observed *in situ* at different stages of crack growth. Observations were made using a Leica binocular or a Keyence numerical microscope by transparency.

Examples of experimental images are shown in Figs. 1(a)–1(g) for K_{III}/K_I values of 0.3 and 0.5 corresponding to initial notch angles of 30° and 45° , respectively. Those images reveal several important features. First, facets have a finger shape with curved tips and flat sides that is consistent with the shape predicted by phase-field simulations [Fig. 1(i) and Movie 1 of [30]]. Second, facets form for values of K_{III}/K_I both below and above the linear stability threshold predicted by Eq. (2), $(K_{III}/K_I)_c \approx 0.39$ for $\nu = 0.38$ of Plexiglas. Within optical resolution, only energetically favored type A facets are observed to emerge from the parent crack with a well-defined tilt angle θ from the original fracture plane. Third, facets coarsen by elimination of other facets, leading to an increase of both facet width and facet spacing along the array with increasing propagation length. Coarsening is clearly visible from top views in Fig. 1(b) and in the sequence Figs. 1(c)–1(e), which moreover shows that surviving facets maintain the same angle while overgrowing others. Additional views are given in Ref. [30].

Simulations were performed with a phase-field model that regularizes stress-field divergences on a process zone scale $\sim \xi$ around the crack front. All energy dissipation takes place on a characteristic time scale τ [41]. Since we are primarily interested in modeling crack evolution in a region away from the experimental sample boundaries where K_{III}/K_I is approximately uniform [19,32], we carried out simulations in a rectangular slab geometry of length D_x , width D_y , and height D_z , defined in Fig. 2(b), with the origin defined at the center of the slab. We impose fixed displacements at $y = \pm D_y/2$, $u_y(x, \pm D_y/2, z) = \pm \Delta_y$ (mode I), and $u_z(x, \pm D_y/2, z) = \pm \Delta_z$ (mode III),

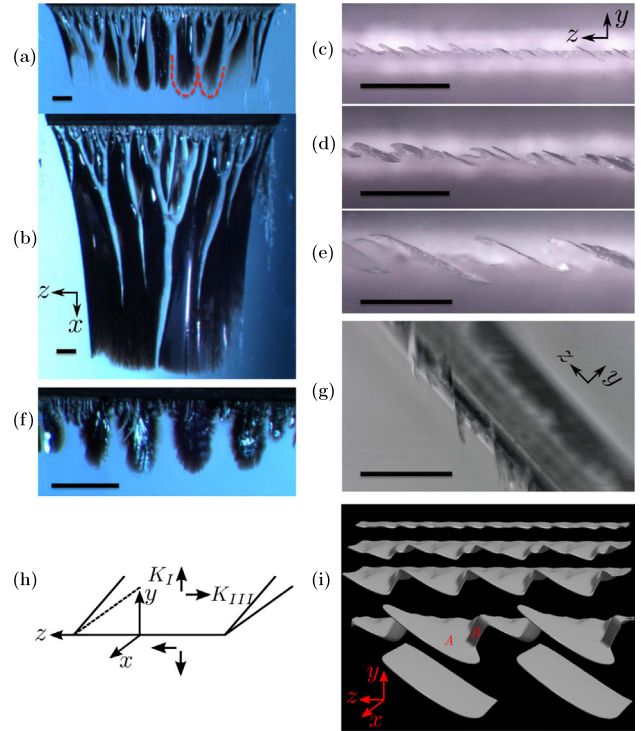


FIG. 1 (color online). *In situ* microscope images (a)–(g) of fatigue cracks in Plexiglas at different stages of crack advance in mixed-mode I + III loading depicted schematically in (h) and corresponding example of crack front segmentation in phase-field simulation (i). $K_{III}/K_I \approx 0.3$ in (a)–(e) and ≈ 0.5 in (f) and (g); (a), (b), and (f) are experimental views from a direction approximately perpendicular to the plane of the parent crack with facets propagating downwards, while views (c), (d), (e), and (g) are views with the crack propagation direction out of the page. Views (c), (d), and (e) correspond to different stages of crack advance increasing from (c) to (e). Broken (pristine) regions of the samples appear in black (light blue) or darker (lighter) gray depending on the viewing direction. The bar scale is 1 mm in all images. The red dashed lines in (a) highlight the curved fronts of two facets as guides to the eye; curved tips are clearly visible in (f). (i) Snapshots of phase-field fracture surfaces ($\phi = 1/2$ surfaces) at different stages of crack advance increasing from top to bottom, showing that energetically favored A facets [18] propagate ahead of B facets, eventually outgrowing them completely. Simulation parameters are $G/G_c = 1.5$, $K_{III}/K_I = 0.5$, and box dimensions $D_x = 307\xi$, $D_y = 100\xi$, and $D_z = 200\xi$.

periodic boundary conditions in z that allow us to model a periodic array of daughter cracks infinite in z [24]. We use a “treadmill” that adds a strained (y, z) layer at $x = D_x/2$ and removes a layer at $x = -D_x/2$ when the crack has advanced by one lattice spacing. This allows us to simulate crack propagation lengths much longer than D_x ($a \gg D_x$), thereby modeling propagation in a slab infinitely long in x [30]. All simulations are performed with $\nu = 0.38$ of Plexiglas. We simulated both quasistatic propagation, where the elastic field is relaxed at each time step of crack advance, and dynamic propagation by solving the full

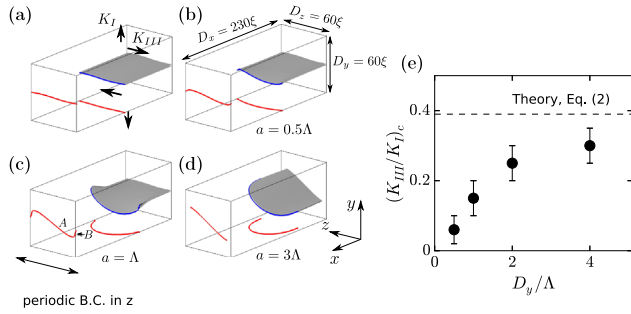


FIG. 2 (color online). Snapshots of phase-field simulations illustrating the destabilization of planar crack growth for $K_{III}/K_I = 0.4$. The crack propagation length a increases from (a) to (d), and both the crack front (blue lines) and its in-plane and out-of-plane projections (red lines) are shown. (e) Plot of linear instability threshold $(K_{III}/K_I)_c$ versus D_y/Λ , where Λ represents the mean facet spacing. Planar growth is unstable (stable) above (below) the filled circles where error bars are defined in Ref. [30]. In all simulations, $G = 1.5G_c$, $D_x = 230\xi$, and $D_z = \Lambda = 60\xi$.

elastodynamic equations. Both sets of simulations yielded similar results for the range $G/G_c \leq 1.5$ where the ratio of the crack propagation speed to the shear wave speed $v/c \leq 0.3$ is small enough to neglect inertial effects [30].

We first carried out simulations to check quantitatively the theoretical prediction of Eq. (2). For this purpose, we slightly perturbed the planar parent crack with a small-amplitude helical perturbation of the form $\delta x_{\text{front}} + i\delta y_{\text{front}} = A_0 e^{-ikz}$, where δx_{front} and δy_{front} indicate the x and y components of deviations of the front from the reference planar crack, respectively, and $k = 2\pi/D_z$ fits one wavelength $D_z = \Lambda$ of the perturbation in the periodic domain in z . The stability of planar crack propagation is then determined by tracking the amplitude of the perturbation that grows or decays exponentially in time [30] if propagation is unstable, as illustrated in Figs. 2(a)–2(d), or stable, respectively. Simulations were carried out by increasing K_{III}/K_I in small steps to determine the threshold $(K_{III}/K_I)_c$ and repeating this procedure for increasing values of D_y/Λ to quantify finite size effects. Figure 2(e) shows that $(K_{III}/K_I)_c$ increases monotonically with D_y/Λ and approaches a value reasonably close to the prediction $(K_{III}/K_I)_c \approx 0.39$ of Eq. (2) in the large system size ($D_y/\Lambda \gg 1$) limit. We checked that instability thresholds reported in Fig. 2(e) remain unchanged within error bars if a random perturbation of the crack front was used instead of a helical perturbation [30]. We conclude that the LEFM theory [Eq. (2)] and phase-field modeling predict similar linear instability thresholds in the large system size limit, even though facets are experimentally observed well below this threshold.

Next, in order to explore the nonlinear character of the bifurcation from a planar to segmented crack front, we measured experimentally the facet tilt angle θ extracted from three-dimensional maps of postmortem fracture surfaces obtained using a profilometer as detailed in Ref. [32].

The angle θ is plotted versus K_{III}/K_I in Fig. 3(a). Furthermore, we investigated computationally the propagation of periodic arrays of A facets in the large system size limit relevant for experiment. We chose $D_y/\Lambda = 2$ based on the results of Fig. 2(e) and an examination of strain fields showing that finite size effects become negligible when $D_y/\Lambda \geq 2$ [30]. We also suppressed coarsening by choosing $D_z = \Lambda$ with periodic boundary conditions along z . In this geometry, we tracked the steady-state branch of propagating solutions by decreasing K_{III}/K_I starting from values above the linear instability threshold to values below this threshold, as low as 0.07 to span the entire experimental range of mode mixity. For each K_{III}/K_I value, we allowed the facet to relax to a new stationary shape and tilt

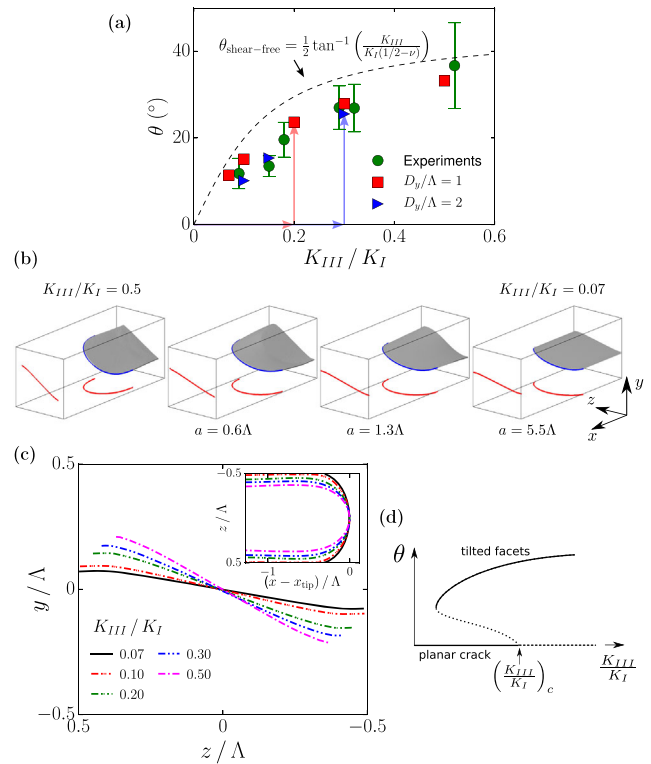


FIG. 3 (color online). (a) Comparison of facet tilt angles obtained from experiments and simulations, where red and blue arrows indicate the instability thresholds of planar crack propagation for $D_y/\Lambda = 1$ and $D_y/\Lambda = 2$, respectively [see Fig. 2(e)], and theoretically predicted assuming shear-free facets (dashed line) [16,24]. (b) Snapshots of a phase-field simulation for $D_y/\Lambda = 1$ demonstrating the subcritical nature of the bifurcation from a planar to segmented crack propagation. A segmented front solution for $K_{III}/K_I = 0.5$ ($\theta = 31^\circ$) was used as an initial condition in a simulation for $K_{III}/K_I = 0.07$, causing the facet angle to relax to a lower steady-state value ($\theta = 11.2^\circ$) (see Movie 2 of [30]). (c) Out-of-plane and in-plane (inset) crack front projections. In all simulations, $D_x = 154\xi$, $D_y = D_z = 60\xi$, $\Lambda = 60\xi$, and $G = 1.5G_c$. (d) Schematic diagram of subcritical bifurcation recapitulating the experimental and simulation results with solid (dashed) lines representing stable (unstable) solutions.

angle, as illustrated in Fig. 3(b) for a simulation where K_{III}/K_I was decreased from 0.5 to 0.07. The computed tilt angles are compared to experimental results in Fig. 3(a) with the corresponding facet shapes shown in Fig. 3(c). Both the facet shapes, which gently curve at their extremities in the yz plane due to elastic interactions between neighboring facets, and the tilt angles are in good quantitative agreement with experimental observations within measurement errors. Figure 3(a) also shows that computed tilt angles are weakly dependent on system size (D_y/Λ) and fall below the prediction of a simple theory, which assumes that facets are shear-free [16,24]. Those results demonstrate that propagating segmented front solutions exist over the entire range of K_{III}/K_I investigated experimentally, including values less than $(K_{III}/K_I)_c$. We conclude that the bifurcation from a planar to segmented front is strongly subcritical, with bistability of planar and segmented crack growth for $K_{III}/K_I < (K_{III}/K_I)_c$ as illustrated schematically in Fig. 3(d).

To characterize coarsening in phase-field simulations, we investigated the stability of a periodic array of facets by repeating the above series of simulations with several facets, corresponding to $D_z = n\Lambda$ with $n \geq 2$. This geometry is motivated by the striking similarity between the coarsening behavior of facets in the present experiments [Figs. 1(a)–1(g)] and coarsening of curved fronts in other interfacial pattern forming systems, in particular, viscous fingering [42] and dendritic crystal growth [43,44]. In those systems, coarsening of finger arrays is associated with a

spatial period-doubling linear instability of the array [43,44]. While longer wavelength perturbations of the array can also be unstable, period doubling leading to the elimination of one of every two fingers in the array is generically the fastest growing mode. Results of simulations for $n = 2$ in Fig. 4(a) show that arrays of facets exhibit a similar period-doubling instability driven by elastic interactions between facets. We have checked that period doubling is the fastest growing mode by also performing simulations with $n > 2$ [30]. This instability yields an increase (decrease) of the SIF and hence the energy release rate at the tips of leading (lagging) facets. The amplification rate of instability is obtained by computing the difference of x -tip position $\Delta x_{\text{tip}}(t)$ between leading and lagging facets, which grows exponentially in time starting from an infinitesimal perturbation, $\Delta x_{\text{tip}}(t) \approx \Delta x_{\text{tip}}(0)e^{\omega v_0 t/\Lambda}$, where v_0 and Λ are the initial facet growth velocity and spacing, respectively. The slopes of semilog plots of $\Delta x_{\text{tip}}(t)/\Lambda$ versus $v_0 t/\Lambda$ in Fig. 4(b) yield values of ω that increase markedly with K_{III}/K_I , showing that a larger mode III component leads to a faster elimination rate of facets.

Coarsening, clearly visible in Fig. 1(b) and other experimental views [30], was quantified experimentally by analyzing postmortem fracture surfaces [32]. The results show that the relation between the mean facet spacing Λ and the crack propagation length a is approximately linear, with a mean slope $\beta \equiv d\Lambda/da$ increasing with K_{III}/K_I [inset in Fig. 4(b)]. To relate the coarsening rates in phase-field simulations and experiments, we derive a simple evolution equation for the average array spacing Λ based on a dynamical mean-field picture as previously done for dendritic arrays [43]. The coarsening rate $\beta \equiv d\Lambda/da \approx \Delta\Lambda/\Delta a$, where $\Delta\Lambda$ is the change of array spacing due to the elimination of one of every two facets along the array or $\Delta\Lambda \approx \Lambda$, while Δa is the distance that the facets propagated during the elimination process. Since elimination occurs via the exponential amplification of small perturbations, facets will propagate an average distance $\Delta a \sim \Lambda/\omega$ during this process, yielding the prediction $\beta \sim \omega$, or $\beta = C\omega$, where C is a constant prefactor of the order of unity. The comparison in the inset in Fig. 4(b) shows that this simple theory is able to predict reasonably well the increase of the coarsening rate with K_{III}/K_I up to the value of the constant prefactor $C = 0.198$ determined from a global best fit to the experimental data for all K_{III}/K_I values.

The reasonably good quantitative agreement between simulated and observed morphologies suggests that LEFM is an adequate theory to describe complex geometrical features of both brittle and fatigue cracks in mixed-mode I + III fracture. Going beyond linear stability analysis, the present results show that the subcritical propagation of segmented cracks is theoretically possible. Nevertheless, they do not identify the mechanism and scale of subcritical facet formation. As suggested by a recent LEFM analysis, material imperfections may contribute to this process [45].

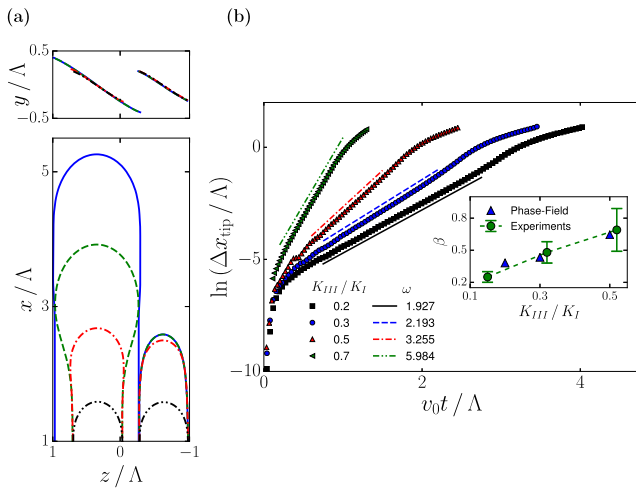


FIG. 4 (color online). (a) Illustration of spatial period-doubling instability in a phase-field simulation for $K_{III}/K_I = 0.5$; out-of-plane and in-plane projections of crack fronts are plotted in the top panel and the bottom panel, respectively (see Movie 3 of [30]). (b) Semilog plot of difference of tip positions along the propagation x axis between leading and lagging facets versus scaled time for different K_{III}/K_I . Inset: Coarsening rate β versus K_{III}/K_I obtained from experiments and phase-field simulations. In all simulations, $D_x = 307\xi$, $D_y = 60\xi$, $D_z = 120\xi$, $\Lambda = 60\xi$, and $G = 1.5G_c$.

However, this scenario, and even more fundamentally the ability of LEFM to model subcritical facet formation, remain to be explored both computationally and experimentally.

The research at Northeastern University was supported by Grant No. DE-FG02-07ER46400 from the U.S. Department of Energy, Office of Basic Energy Sciences and a seed grant from the Massachusetts Green High Performance Computing Center. The research at University Paris Sud benefited of financial support from ANR GeoSMEC (2012-BS06-0016-03). The research at Polytechnic University of Catalonia was supported by the Ministerio de Economía y Competitividad of Spain and FEDER through research Project No. FIS2012-37655-C02-01. The authors thank L. Auffray, D. Bonamy, F. Buchholz, V. Doquet, J.-C. Eytard, R. Pidoux, and A. Tanguy for their help in the experiments and J.-B. Leblond for helpful discussions.

*ch.chen@neu.edu

†a.karma@neu.edu

- [1] E. Bouchbinder, J. Fineberg, and M. Marder, *Annu. Rev. Condens. Matter Phys.* **1**, 371 (2010).
- [2] A. Yuse and M. Sano, *Nature (London)* **362**, 329 (1993).
- [3] O. Ronsin, F. Heslot, and B. Perrin, *Phys. Rev. Lett.* **75**, 2352 (1995).
- [4] G. Gauthier, V. Lazarus, and L. Pauchard, *Europhys. Lett.* **89**, 26002 (2010).
- [5] C. Maurini, B. Bourdin, G. Gauthier, and V. Lazarus, *Int. J. Fract.* **184**, 75 (2013).
- [6] B. Bourdin, J.-J. Marigo, C. Maurini, and P. Sicsic, *Phys. Rev. Lett.* **112**, 014301 (2014).
- [7] T. Baumberger, C. Caroli, D. Martina, and O. Ronsin, *Phys. Rev. Lett.* **100**, 178303 (2008).
- [8] E. Sommer, *Eng. Fract. Mech.* **1**, 539 (1969).
- [9] W. G. Knauss, *Int. J. Fract.* **6**, 183 (1970).
- [10] K. Palaniswamy and W. G. Knauss, in *Mechanics Today*, edited by Nemat-Nasser (Pergamon, New York, 1975), Vol. 4, pp. 87–148.
- [11] F. Hourlier and A. Pineau, *Mem. Sci. Rev. Metall.* **76**, 175 (1979).
- [12] D. D. Pollard, P. Segall, and P. T. Delaney, *Geol. Soc. Am. Bull.* **93**, 1291 (1982).
- [13] S. Suresh and E. K. Tscheegg, *J. Am. Ceram. Soc.* **70**, 726 (1987).
- [14] D. D. Pollard and A. Aydin, *Geol. Soc. Am. Bull.* **100**, 1181 (1988).
- [15] J. R. Yates and K. J. Miller, *Fatigue Fract. Eng. Mater. Struct.* **12**, 259 (1989).
- [16] M. L. Cooke and D. D. Pollard, *J. Geophys. Res.* **101**, 3387 (1996).
- [17] V. Lazarus, Ph.D. thesis, Université Pierre et Marie Curie (Paris VI), France, 1997.
- [18] V. Lazarus, J. B. Leblond, and S. E. Mouchrif, *J. Mech. Phys. Solids* **49**, 1421 (2001).
- [19] V. Lazarus, F. G. Buchholz, M. Fulland, and J. Wiebesiek, *Int. J. Fract.* **153**, 141 (2008).
- [20] B. Lin, M. E. Mear, and K. Ravi-Chandar, *Int. J. Fract.* **165**, 175 (2010).
- [21] R. V. Goldstein and N. M. Osipenko, *Dokl. Phys.* **57**, 281 (2012).
- [22] K. H. Pham and K. Ravi-Chandar, *Int. J. Fract.* **189**, 121 (2014).
- [23] O. Ronsin, C. Caroli, and T. Baumberger, *Europhys. Lett.* **105**, 34001 (2014).
- [24] A. J. Pons and A. Karma, *Nature (London)* **464**, 85 (2010).
- [25] J. B. Leblond, A. Karma, and V. Lazarus, *J. Mech. Phys. Solids* **59**, 1872 (2011).
- [26] J. B. Leblond, V. Lazarus, and A. Karma, *Int. J. Fract.* **191**, 167 (2015).
- [27] A. A. Griffith, *Phil. Trans. R. Soc. A* **221**, 163 (1921).
- [28] V. Hakim and A. Karma, *J. Mech. Phys. Solids* **57**, 342 (2009).
- [29] R. V. Goldstein and R. L. Salganik, *Int. J. Fract.* **10**, 507 (1974).
- [30] See Supplemental Material at <http://link.aps.org/supplemental/10.1103/PhysRevLett.115.265503>, which includes Refs. [24,25,28,31–38,41], for details of the experiments and phase-field simulations and movies.
- [31] G. Pulos and W. Knauss, *Int. J. Fract.* **93**, 145 (1998).
- [32] T. Cambonie and V. Lazarus, *Procedia Mater. Sci.* **3**, 1816 (2014).
- [33] S. Melin, *Int. J. Fract.* **23**, 37 (1983).
- [34] M. L. Fender, F. Lechenault, and K. E. Daniels, *Phys. Rev. Lett.* **105**, 125505 (2010).
- [35] A. Karma and A. E. Lobkovsky, *Phys. Rev. Lett.* **92**, 245510 (2004).
- [36] H. Henry and H. Levine, *Phys. Rev. Lett.* **93**, 105504 (2004).
- [37] H. Henry and M. Adda-Bedia, *Phys. Rev. E* **88**, 060401 (2013).
- [38] H. Henry, *Europhys. Lett.* **83**, 16004 (2008).
- [39] F.-G. Buchholz, A. Chergui, and H. A. Richard, *Eng. Fract. Mech.* **71**, 455 (2004).
- [40] W. Linning, in *Mixed-Mode Fatigue and Fracture (ESIS 14)*, edited by H. P. Rossmannith and K. J. Miller (Professional Engineering Publishing, London, 1993), pp. 201–215.
- [41] A. Karma, D. A. Kessler, and H. Levine, *Phys. Rev. Lett.* **87**, 045501 (2001).
- [42] D. A. Kessler and H. Levine, *Phys. Rev. A* **33**, 3625 (1986).
- [43] J. A. Warren and J. S. Langer, *Phys. Rev. E* **47**, 2702 (1993).
- [44] W. Losert, B. Q. Shi, H. Z. Cummins, and J. A. Warren, *Phys. Rev. Lett.* **77**, 889 (1996).
- [45] J.-B. Leblond and V. Lazarus, *J. Mech. Mater. Struct.* **10**, 299 (2015).